Title

High Selectivity and Activity of Ti-Cu(111) Dilute Alloys for the Deoxygenation of Ethanol to Ethylene

Authors

Shi, Junjie
Ngan, Hio Tong
Sautet, Philippe
et al.

Publication Date

2023-08-21

DOI

10.1021/acscatal.3c02530

High selectivity and activity of Ti-Cu(111) dilute alloys for the deoxygenation of ethanol to ethylene

Junjie Shi[1,†], Hio Tong Ngan[2,†], Philippe Sautet[2,3*] and Jason F. Weaver[1*]

[1]Department of Chemical Engineering, University of Florida, Gainesville, FL 32611, USA

[2]Department of Chemical and Biomolecular Engineering, University of California, Los Angeles, Los Angeles, California 90095, USA

[3]Department of Chemistry and Biochemistry, University of California, Los Angeles, Los Angeles, California 90095, USA

[†]Junjie Shi and Hio Tong Ngan contributed equally to this work.

Corresponding author emails:

*sautet@ucla.edu

*weaver@che.ufl.edu

Abstract

Dilute Ti-Cu(111) alloys are found to be highly selective for converting ethanol to ethylene. Temperature programmed reaction spectroscopy (TPRS) shows that adsorbed ethanol deoxygenates on Ti-Cu(111) surfaces with ~10% Ti to produce gaseous C_2H_4 and H_2 at temperatures near 400 K. Scanning tunneling microscopy and vibrational spectroscopy of adsorbed CO demonstrate that Ti surface sites are oxidized to TiO_x by reaction with ethanol, causing the reaction selectivity to change from C_2H_4 to acetaldehyde production during repeated TPRS experiments with ethanol. TPRS simulations derived from density functional theory (DFT) calculations confirm that Ti ensembles within the Cu(111) surface layer promote ethanol deoxygenation at moderate temperature, and reveal a significant enhancement in the activity and selectivity for gaseous C_2H_4 and H_2 production as the Ti ensemble size is increased from monomer to trimer. DFT shows that increasing the Ti_n ensemble size from n = 1 to 3 increases the stability of the adsorbed O-atom released during C-O bond cleavage, thus facilitating ethanol deoxygenation. The calculations show that the O-atom bound to Ti further enhances C_2H_4 production by destabilizing the adsorbed C_2H_4 and its dehydrogenation product, and that this destabilization effect becomes more pronounced as the Ti ensemble size is increased from monomer to trimer. Our results demonstrate that dilute Ti-Cu(111) alloys promote the conversion of ethanol to ethylene at moderate temperature, and reveal that this surface chemistry is strongly influenced by the Ti ensemble size and the adsorbed O-atom released during C-O cleavage.

Keywords: Ti-Cu(111), dilute alloys, ethanol, deoxygenation, alcohol dehydrogenation, HDO

Introduction

Dilute alloys have attracted considerable attention as catalysts due to their ability to promote selective chemical transformations.[1-5] The general strategy for synthesizing a dilute alloy catalyst is to disperse a transition metal within the surface of a coinage metal (Cu, Ag, Au) so that the transition metal exists as atomic-scale ensembles in a less reactive host metal. Single-atom alloys (SAAs) represent a special class of dilute alloy catalysts as the transition metal is present as individual atoms within the coinage metal surface.[2] The transition metal ensembles serve as reactive centers for adsorbed molecules and their low nuclearity can promote selective chemistries in part by suppressing multi-step routes toward undesirable products. Fundamental studies of dilute alloy catalysts have focused mainly on late transition-metals (Pd, Pt, Rh, Ni) as the active sites, and indeed demonstrate that these materials are selective catalysts for a wide range of chemistries, particularly hydrogenation and dehydrogenation reactions.[2, 6-12]

Dilute alloy catalysts with early transition-metal dopants have received less attention yet may afford opportunities for converting organic oxygenates to more valuable products. The high oxophilicity of early transition metals can lead to preferential activation and functionalization of O-containing functional groups (O-H, C-O) of organic compounds, enabling chemistries such as the selective hydrogenation of unsaturated aldehydes to alkenols[13] and hydrodeoxygenation (HDO) reactions for the conversion of alcohols to olefins as well as upgrading of biomass-derived compounds.[14] The low nuclearity of atomic ensembles of early transition metals could also hinder undesirable reaction steps after initial C-O activation as well as facilitate the hydrogenation of oxygen released during reaction to H_2O. In support of these ideas, a recent study demonstrates that

PtCo catalysts are highly selective in converting 5-hydroxymethylfurfural to dimethylfuran,[15] while computational screening investigations have identified alloys with various early transition metals doped into Pt(111) and Ni(111) as promising candidates for the HDO of phenol to benzene.[16-17] A more recent investigation has shown that Cr-rich atomic-scale PtCr ensembles dispersed in the Ag(111) surface are highly selective in converting ethanol to ethylene during temperature programmed reaction spectroscopy (TPRS).[18] These prior results indeed support the idea that dilute alloys with early transition-metal dopants have potential to catalyze HDO reactions to convert organic oxygenates to more valuable products.

The present study focuses on Ti-Cu(111) surfaces as a representative dilute alloy derived from an early transition metal. We have recently shown that single-atom alloys can be generated by depositing Ti onto Cu(111) at temperatures above ~500 K in ultrahigh vacuum (UHV), whereas Cu-covered, Ti-containing islands are formed during deposition at lower temperature.[19] This growth behavior enables investigations of the chemical properties of Ti-Cu(111) surfaces with distinct Ti structures. Although such studies have not yet been reported, recent work shows that nanoporous (np) TiCu alloys are significantly more active than pure np-Cu in promoting H_2/D_2 exchange, thus revealing the potential of np-TiCu for promoting catalytic hydrogenation reactions.[20]

Here, we show that Ti-Cu(111) surfaces are highly active and selective in promoting the deoxygenation of ethanol to ethylene, with Ti at the surface becoming oxidized during TPRS. We present evidence that Ti dimers and trimers are significantly more reactive toward ethanol than Ti monomers, and that the oxygen released to Ti destabilizes the adsorbed C_2H_4 product and promotes its desorption. Our results provide insights for understanding how the sizes of atomic Ti_n ensembles

(n = 1 to 3) as well as the oxygen released by C-O bond cleavage serve to promote the deoxygenation of ethanol to ethylene on Ti-Cu(111) surfaces.

Experimental Details

All experiments were performed in an ultrahigh vacuum (UHV) system described previously.[21] The UHV chamber is pumped by turbo, ion and titanium sublimation pumps and maintained a base pressure of 2×10^{-10} Torr. The chamber is equipped with a scanning tunneling microscope (RHK), a four-grid retarding field analyzer (SPECS) for low-energy electron diffraction (LEED) and Auger electron spectroscopy (AES), a quadruple mass spectrometer (QMS) (Hiden), a Fourier transform infrared spectrometer system (Bruker, Tensor 27), an ion sputter gun, and an electron-beam metal evaporator (McAllister Technical Services) for vapor deposition of Ti.

The Cu (111) crystal used for the STM study is a circular top-hat shaped disk (10 × 1.65 mm) cut to isolate the (111) surface plane within a tolerance of ± 0.1°. Details of the sample support structure and cleaning procedure have been reported previously.[22] In general, the sample was cleaned by multiple alternating cycles of Ar^+ (2.0 keV) sputtering at 300 K followed by thermal annealing at 750 K. The cleanliness of sample was ascertained from AES and observation of a sharp LEED pattern characteristic of Cu(111).

Metallic Ti was deposited onto the Cu(111) sample using an electron beam evaporator fitted with a Ti rod. Evaporation was performed in UHV with the sample held at constant temperatures between 300 and 700 K. AES spectra showed that negligible amounts of impurities, particularly C and O, were present on the sample after Ti deposition. The Ti coverage was calibrated by collecting AES spectra as

a function of Ti exposure to clean Cu (111) at 300 K and relating the intensity of the Ti LMM peak at 387 eV to the intensity of the Cu LMM peak at 920 eV following the equation as below:

$$\text{Ti-coverage (ML)} = I_{Ti}/S_{Ti}/(I_{Ti}/S_{Ti} + I_{Cu}/S_{Cu})$$

where I_{Ti} and I_{Cu} represent the intensities of the Ti LMM and Cu LMM peaks and S_{Ti} and S_{Cu} represent the AES sensitivity factors for Ti and Cu, with values of 0.44 and 0.21, respectively.[23] The average Ti deposition rate was 0.027 ML/min for our measurements, where 1 ML is defined as the surface atom density of Cu(111). We also estimated the Ti coverage by calculating the area covered by Ti-containing islands observed in STM images acquired after depositing Ti below ~400 K. We assume that the fractional area covered by the islands is representative of the Ti coverage for low temperature deposition. The average Ti deposition rate estimated from the STM analysis is ~0.02 ML/min which agrees reasonably well with that estimated from the AES measurements. The experiments reported in this study were mainly performed after depositing ~0.10 ML of Ti onto Cu(111) at temperatures of 300 K and 600 K.

TPRS experiments were performed using a circular Cu(111) single crystal (10 mm × 2 mm). The sample was attached to two 0.40 mm tungsten wires mounted onto an LN2 cooled sample holder. A type K thermocouple was pressed into a 0.5 mm diameter hole in the side of the sample for temperature measurements. Ethanol was purified with multiple freeze-pump-thaw cycles and dosed onto the sample surface using a variable leak valve. After dosing ethanol at 90 K, TPRS spectra were collected by heating to 700 K at a rate of 1 K/s. The signals of six masses (m/z = 2 (H_2), 18 (H_2O), 28 (C_2H_4), 29 (CHO), 31 (CH_3O), 32 (O_2) and 44 (CO_2)) were monitored during the TPRS experiments. Mass fragment m/z = 31 is the dominant component in the ethanol cracking pattern and was monitored

to determine the desorption rate of ethanol. The TPRS traces for acetaldehyde were generated by subtracting the ethanol contributions from the trace of m/z = 29. Ethylene desorption was monitored from the m/z = 28 fragment. Confirmation that only C_2H_4 contributed to the m/z = 28 trace in these experiments was obtained by observing close overlap among the desorption traces of m/z = 26, 27 and 28 after scaling them according to the C_2H_4 fragmentation pattern. The desorption rates of O_2, H_2O and H_2 were monitored by measuring their parent ions, m/z = 32, 18 and 2, respectively, during TPRS. Product desorption yields were estimated from TPRS traces and are referenced to the saturation coverage of an ethanol monolayer on pure Cu(111), after applying relative sensitivity factors. The desorption yields are given in units of ML (monolayer), where 1 ML is defined as the amount of ethanol in a saturated monolayer on pure Cu(111) as determined from TPRS measurements.

STM measurements were performed at a sample temperature of ~300 K, and the tunneling interaction was set to constant current feedback mode. The equipment used for STM was produced by RHK and includes an UHV 300 "beetle-type" scan head operated with a scanning probe microscope (SPM) 100 controller. Images were collected at typical scan settings in the range of +0.08 to +0.5 V sample bias and tunneling currents of 0.4–1.2 nA. Feature heights estimated from STM line scans were calibrated to the Cu(111) monatomic step height of 0.210 nm. Reflection absorption infrared spectroscopy (RAIRS) measurements were performed by reflecting a non-polarized IR beam from the sample at an incident angle of ~80° from the surface normal and detecting the reflected beam using an external liquid-nitrogen cooled MCT detector. All the reported RAIRS spectra are an average of 512 scans and were collected at 4 cm^{-1} resolution.

Computational Details

All DFT calculations were performed using the Vienna ab initio simulation package (VASP).[24-27] The dDsC-dispersion-corrected PBE functional and a plane-wave basis set with a cutoff energy of 450 eV were employed for all calculations reported in this study.[28-29] Standard PAW pseudopotentials were used for all elements except Ti for which the version '_sv', with 12 electrons in the valence, was used. Ti-Cu(111) metal surfaces were modeled using a four-layer slab and a (3 · 3) unit cell. For this unit cell size, a Monkhorst-Pack-generated 5 · 5 · 1 K-point grid was used. During structural optimizations, the bottom two layers of the slab were fixed in the Cu bulk positions, while the upper two layers and the surface adsorbates were allowed to relax. These optimizations were stopped when the force convergence criterion of 0.02 eV/Å was reached. Density-of-states calculations were performed using the Local Orbital Basis Suite Towards Electronic Structure Reconstruction (LOBSTER).[30] Transition states were located using both the climbing image nudged elastic band (CI-NEB) and dimer methods.[31-32] VESTA was used to visualize all atomic configurations.[33]

Results and discussion

Initial Ti structure and morphology on Cu(111): Islands vs. dilute alloy

The reactivity of Ti-containing islands on Cu(111) and a dilute Ti-Cu(111) alloy was investigated in the present study. Recently, our groups have used STM, RAIRS of adsorbed CO and DFT calculations to characterize the structures that form during Ti deposition on Cu(111), and shown that Cu-covered, Ti-containing islands form during Ti deposition at 300 K while a dilute Ti-Cu(111) surface alloy forms during deposition above 500 K.[19] The DFT calculations reported in that study

accurately reproduce the differences in C-O stretch frequencies assigned to CO adsorbed on surface Ti_1 sites of Ti-Cu(111) alloys vs. Cu-Ti_n-Cu(111) subsurface alloy structures, thus lending support to our structural interpretations. As shown in Figure 1a, Ti deposition at 300 K preferentially generates Ti-containing islands at the ascending step edges of Cu(111) as well as larger islands that are sparsely distributed on the terraces. Islands of pure Cu are also generated at descending step edges (see below) due to the place exchange that occurs when Ti incorporates into the Cu step edge. A large fraction of the Ti-containing islands is covered by a Cu single layer and gives rise to a characteristic C-O stretch band at about 2104 cm^{-1} in RAIR spectra obtained after CO adsorption (Figure 1b).[19] Adsorbed CO on low-coordination Cu sites (steps, kinks) also contributes to the spectral intensity observed at frequencies higher than the band arising from CO on Cu(111) terraces (2075 cm^{-1}).[34-36] Slightly weaker binding causes the CO coverage on Cu(111) terraces to decrease more sharply with increasing temperature compared with CO on the Cu-Ti islands. As a result, the peaks from CO adsorbed on the islands vs. terraces exhibit similar intensities in spectra acquired at 160 K even though islands are present in lower coverages (Figure 1c). Contiguous Ti ensembles may also be exposed at the surface or edges of the islands, but such structures do not produce a distinct CO RAIRS band. According to DFT, adsorbed CO preferentially adopts a flat-lying geometry on surface Ti ensembles with more than one Ti atom and would thus be difficult to detect with RAIRS due to the surface selection rule.[19]

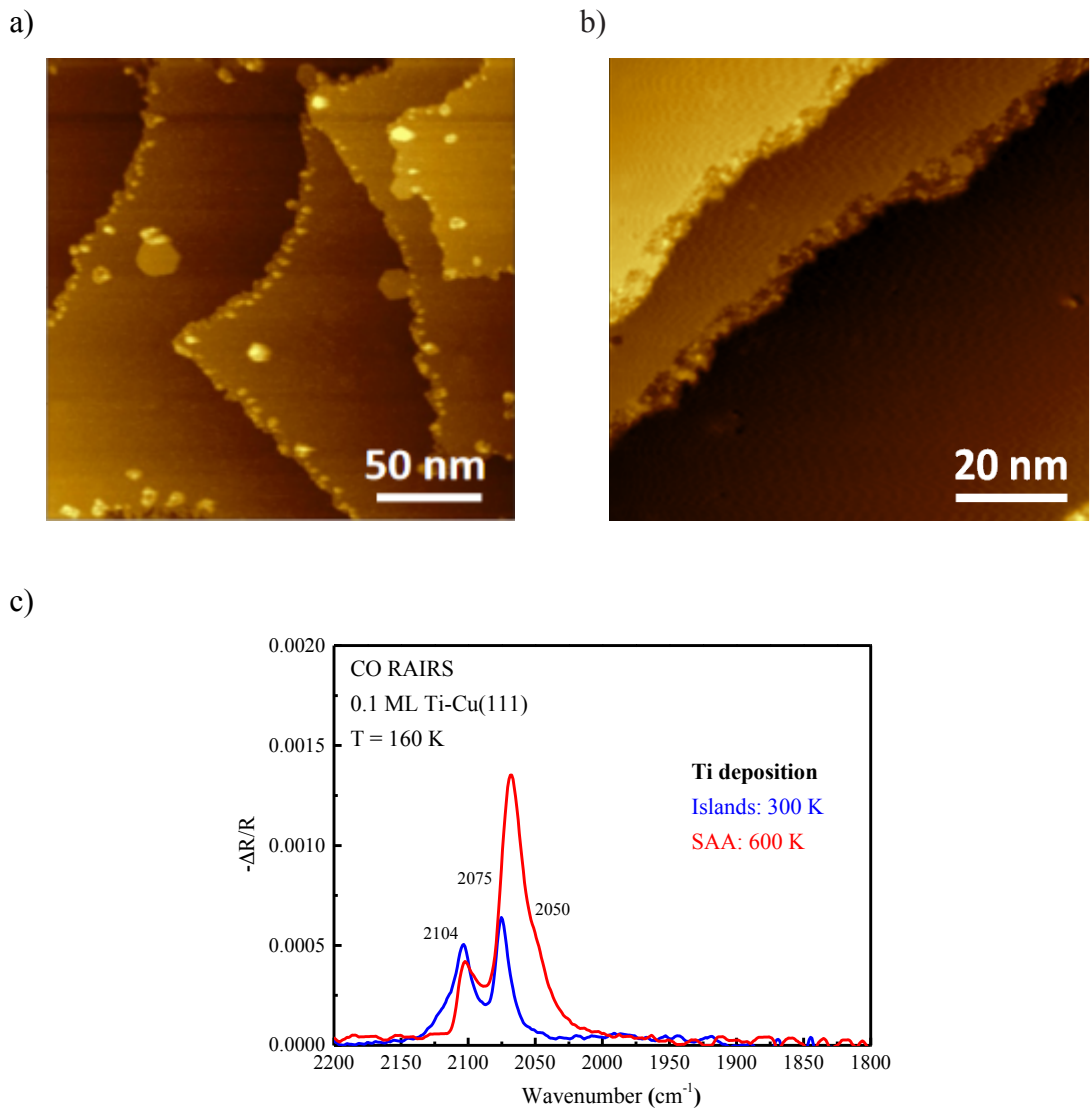

Figure 1. Representative STM images obtained after depositing ~0.1 ML of Ti on Cu(111) at 300 K and 600 K to generate, respectively, a) Ti-containing islands and b) a Ti-Cu(111) alloy. c) RAIRS spectra collected after adsorbing CO to saturation on the island-covered surface (blue) and the Ti SAA (red) at 160 K.

Deposition at 600 K promotes Ti alloying into Cu(111) as evidenced by pitting and roughening of the ascending step edges and the absence of islands at the steps (Figure 1b). Single-atom alloy sites of Ti in Cu(111) generate a distinct CO RAIRS band at 2050 cm^{-1} (Figure 1c).[19] After depositing

~0.1 ML of Ti, the intensity of the 2075 cm^{-1} peak, arising from CO on Cu(111) terraces, is more than two times higher in spectra collected at 160 K from the Ti-Cu(111) SAA surface compared with the Ti-containing island covered surface. This may result from intensity transfer from CO adsorbed on Ti SAA sites to CO adsorbed on nearby Cu(111) terrace sites.[37] Determining the origin of this effect requires further investigation that lies outside the scope of the present study but is unnecessary for accomplishing the goals of the present study. The ratio of CO peaks at 2104 and 2075 cm^{-1} is lower in the RAIR spectra acquired after depositing Ti at 600 K compared with 300 K (Figure 1c), further demonstrating that alloying is favored over island formation during Ti deposition at elevated temperature.

Initial reactivity of Ti islands vs. dilute alloy on Cu(111)

Our experiments corroborate earlier work showing that terraces on pure Cu(111) are unreactive toward ethanol during TPRS whereas step edges promote ethanol dehydrogenation to acetaldehyde.[38] For pure Cu(111), negligible reactivity was observed during TPRS when the surface was annealed at 700 K prior to ethanol adsorption (Fig. S1). However, sputtering at 600 K without subsequent annealing enhances the reactivity of pure Cu(111) toward ethanol. For such a sputtered surface, we find that ethanol dehydrogenation produces small acetaldehyde and H_2 peaks at 325 and 360 K during TPRS (Fig. S1); no other reaction products were observed. Since the Cu(111) sample was annealed above 700 K prior to Ti deposition, our experiments suggest that pure Cu sites would contribute negligibly to the reactivity of the Ti-Cu(111) surfaces investigated here.

The initial Ti-Cu(111) surfaces investigated in this study promote the deoxygenation of ethanol to

gaseous C_2H_4 and H_2 during TPRS. As seen in Fig. 2a, C_2H_4 and H_2 desorb concurrently in a TPRS peak near 370 K after ethanol is adsorbed to saturation on the surface with Ti-containing islands. In this experiment, the yield of C_2H_4 is equal to roughly 9% of the ethanol saturation coverage on pure Cu(111). No acetaldehyde or other C-containing reaction products were detected using TPRS. Further, other than unreacted ethanol, no other gaseous products containing oxygen were detected, suggesting that the ethanol deoxygenation reaction generated O-atoms that remained on the surface. These results show that Ti-containing islands on Cu(111) promote the deoxygenation of ethanol at moderate temperature to selectively generate C_2H_4 and H_2.

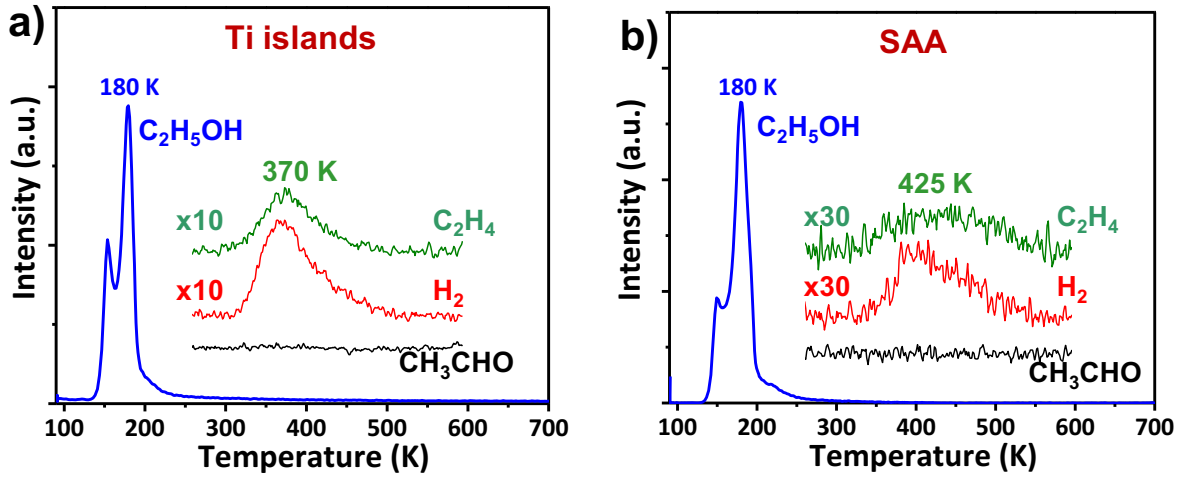

Figure 2. TPRS traces of C_2H_5OH (blue), C_2H_4 (green), H_2 (red) and CH_3CHO (black) obtained from Ti-Cu(111) surfaces with ~0.1 ML of Ti in the form of a) Ti-containing islands and b) Ti alloy sites. Ethanol was adsorbed at 90 K in a quantity sufficient to saturate the monolayer state.

The Ti-Cu(111) SAA surface also promotes ethanol deoxygenation to C_2H_4 and H_2 but the yields are almost three times lower compared with the Ti-Cu(111) surface covered with Ti-containing islands. For the Ti-Cu(111) SAA, the C_2H_4 and H_2 TPRS peaks are broad and centered at about 425

K, which is a higher temperature than that seen from the Ti-containing islands (Fig 2a-b). Quantifying the density of Ti sites on the island-covered surface vs. the Ti-Cu(111) SAA is challenging. A possibility is that the ethanol deoxygenation activity of Ti sites is similar on these surfaces and the lower product yields on the Ti-Cu(111) SAA indicates that this surface had a lower coverage of active Ti sites. Alternatively, these surfaces may have similar coverages of surface Ti sites but the types of Ti sites available on the island-covered surface are intrinsically more active than those on the alloy surface. Below, we present DFT results showing large differences in the reactivity of Ti surface ensembles of varying size toward ethanol. A key finding is that Ti ensembles within the Cu(111) surface are active and highly selective for deoxygenating adsorbed ethanol at moderate temperature.

Change in reactivity of Ti-Cu(111) after repeated ethanol TPRS

The chemical properties of the Ti-Cu(111) surfaces change after successive ethanol TPRS experiments in a manner that is strongly suggestive of Ti oxidation to TiO_x via reaction with ethanol. Fig. 3a shows TPRS traces of C_2H_4, CH_3CHO and H_2 obtained after repeatedly adsorbing ethanol to saturation and performing TPRS on a surface initially prepared by depositing ~0.1 ML of Ti onto Cu(111) at 300 K to generate Ti-containing islands. As shown above, on the initial metallic surface, ethanol selectively converted to gaseous C_2H_4 and H_2 during TPRS, while negligible quantities of acetaldehyde or other products desorbed. In the second TPRS experiment, the C_2H_4 yield is significantly diminished, and acetaldehyde desorbed concurrently with H_2 in a broad TPRS peak at ~425 K. The C_2H_4 TPRS peak also shifted from about 370 K to 510 K after the first TPRS

experiment, suggesting that C_2H_4 production began to occur through a new, higher barrier pathway after the initial deoxygenation of ethanol on the metallic Ti sites. The H_2 TPRS yield decreased with the C_2H_4 yield but settled at a constant value. During the fourth TPRS experiment, C_2H_4 desorption is no longer observed while acetaldehyde and H_2 production persisted at the same yield as observed during the second TPRS experiment. These changes suggest that ethanol deoxygenation during TPRS transforms metallic Ti to TiO_x, with a concomitant shift in the ethanol reaction selectivity from deoxygenation to dehydrogenation.

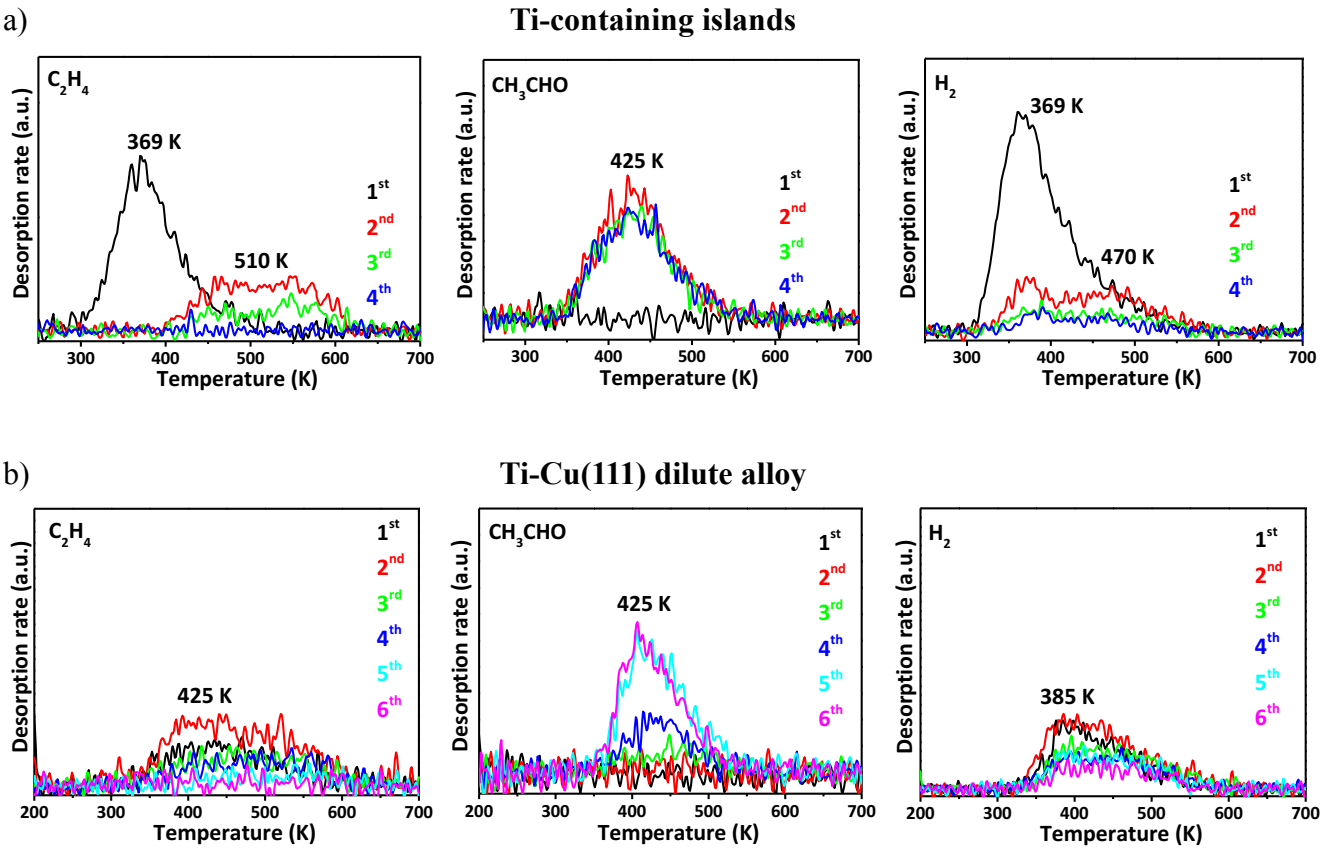

Figure 3. Changes in product distributions during repeated ethanol TPRS experiments on Ti-Cu(111) surfaces. TPRS traces of C_2H_4, CH_3CHO and H_2 (left to right) acquired from a) Ti-containing islands on Cu(111) (top) and b) a Ti-Cu(111) dilute alloy (bottom), each with ~0.1 ML of Ti, after repeatedly saturating the surfaces with an ethanol monolayer at 90 K and heating to 700 K. Sequences of four and six TPRS experiments were sufficient to cause the reactivity to stabilize on the island-covered surface vs. the dilute alloy, respectively.

The reactivity of the dilute Ti-Cu(111) alloy changed during repeated ethanol TPRS experiments in a similar way as seen for the Ti-containing islands. On the initial alloy surface, ethanol selectively deoxygenates producing a broad C_2H_4 TPRS feature centered at about 425 K as well as a broad H_2 peak with a maximum near 385 K (Fig. 3b). During successive TPRS experiments, the C_2H_4 TPRS feature skewed slightly toward higher temperature and diminished into the baseline after about the fifth or sixth experiment. An acetaldehyde TPRS peak at ~425 K became evident during the fourth TPRS experiment and was more intense in the fifth TPRS experiment. The acetaldehyde TPRS yield remained approximately constant in subsequent TPRS experiments. Compared with the Ti-containing islands, the Ti-Cu(111) SAA required more ethanol TPRS experiments to reach a steady reactivity in which C_2H_4 production was negligible and the acetaldehyde yield remained constant. Interestingly, although the initial reactivity differed quantitatively between the Ti-containing islands and the Ti-Cu(111) SAA, the final reactivity achieved after successive TPRS experiments became similar for the two surfaces in that each selectively produced nearly the same quantities of acetaldehyde in a TPRS peak at 425 K. This behavior suggests that similar reactive sites were generated when the active metallic Ti sites on these surfaces (islands vs. alloy) oxidized toward TiO_x during ethanol deoxygenation.

Surface changes after repeated ethanol TPRS

Only a small fraction of surface sites appears to be active for ethanol deoxygenation on Ti-containing islands prepared on Cu(111) at 300 K. STM images acquired from an island-covered

surface appear qualitatively similar before vs. after repeatedly (4x) saturating the surface with ethanol and heating to 700 K. For the images shown in Figure 4a, the coverage of islands and their average size remain near ~10% and ~8 nm, respectively, after the reactive ethanol exposures. The island size distributions are relatively broad, with smaller islands decorating the ascending step edges compared with the terraces, but do not exhibit obvious changes after ethanol reacts on the surface. Our TPRS experiments show that repeatedly reacting ethanol on the island-covered surface changes the surface reactivity in a way that is consistent with Ti oxidation to TiO_x. The fact that the accompanying changes in surface morphology are minor suggests that only a small fraction of surface sites were initially active toward the deoxygenation of ethanol and modified by this reaction.

a)

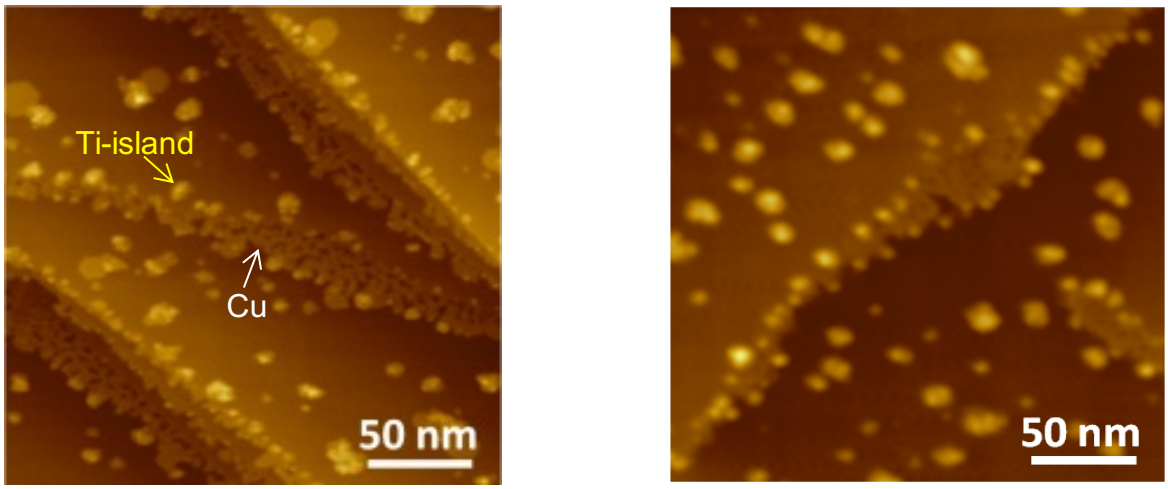

b)

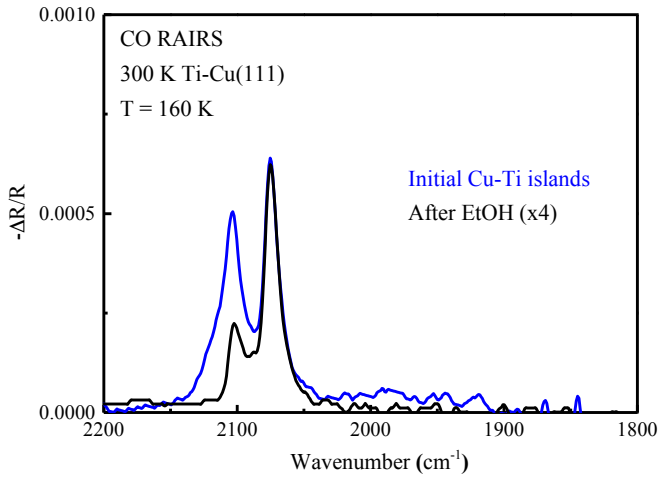

Figure 4. a) STM images obtained from Cu(111) covered with Ti-containing islands before (left) and after (right) four successive ethanol TPRS experiments. A Ti-containing island and a roughened Cu region at an ascending and descending step edge, respectively, are highlighted in the image on the left. b) CO RAIRS spectra acquired at 160 K before and after repeated (4x) ethanol TPRS on a Ti-island covered Cu(111) surface.

Changes in CO RAIR spectra observed after the reactive ethanol exposures are suggested to arise from thermal healing of defect-laden Cu domains which are present after Ti deposition at 300 K. Firstly, RAIRS peaks attributable to CO adsorbed on TiO_x domains were not observed in spectra

acquired after performing repeated ethanol TPRS experiments on the island-covered surface. This is expected because the binding of CO is generally too weak for CO to accumulate in appreciable coverages on TiO_2 domains at 160 K.[39] The CO RAIR spectra acquired after the ethanol exposures do exhibit a significant decrease in the peak intensity at 2104 cm^{-1} (Fig. 4b). While a decrease in the coverage of Cu-covered Ti islands would cause the C-O stretch band at 2104 cm^{-1} to lose intensity, our STM images do not support this interpretation since they show that the density of islands is similar before and after the ethanol exposures (Fig. 4a). We thus suggest that the diminution of the 2104 cm^{-1} peak is associated largely with the elimination of low-coordination Cu sites caused by heating to 700 K rather than structural changes induced by the reactions of ethanol. Our prior work shows that Cu is ejected from step edges during Ti incorporation at 300 K and forms an open network of domains that emanate from the descending step edges (Fig. 4a).[19] STM images exhibit fewer of these roughened Cu domains after the repeated ethanol exposures and heating, suggesting that a fraction of the domains thermally rearranged into the close-packed structure when the surface was heated to 700 K and thereby eliminated low-coordination Cu sites that contribute to the CO RAIRS peak at 2104 cm^{-1}. In support of this interpretation, we find that the RAIRS peak near 2104 cm^{-1} diminishes after briefly annealing an island-covered surface at 700 K, without adsorbing ethanol (Fig. S2).

We suggest that only Ti sites that were initially exposed at the vacuum-solid interface are active in promoting ethanol deoxygenation under TPRS conditions and that Cu-sites over Ti subsurface atoms are inactive. DFT calculations presented below support this interpretation. Given that the morphological changes observed with STM are minor, we speculate that only a small fraction of the

Ti was exposed at the surface, e.g., through voids in the Cu overlayer or at island perimeters, and oxidized to TiO_x during the repeated EtOH TPRS experiments. A prior study shows that sites formed at the interface of TiO_x clusters on Au(111) are active in promoting ethanol conversion to acetaldehyde and ethylene during TPRS,[40] suggesting that analogous interfacial sites may be active in the Ti-Cu(111) system.

Changes in surface properties provide clear evidence that ethanol deoxygenation transforms Ti alloy sites into TiO_x domains. After repeated (6x) ethanol TPRS experiments, STM images show that the step edges of the initial SAA became more smooth and that small clusters (~2 nm) formed, mainly along the ascending step edges (Fig. 5a). These changes are attributed to the oxidation of Ti alloy sites and the formation TiO_x clusters. Consistent with this interpretation, CO RAIRS shows that the characteristic band at 2050 cm^{-1} from Ti_1 sites is completely absent after the reactive ethanol exposures (Fig. 5b). As noted above, a new band associated with CO adsorbed on TiO_x should not be observed in RAIRS spectra collected at 160 K. Thus, the change in surface morphology as well as the CO RAIRS data support the conclusion that Ti alloy sites are active for ethanol deoxygenation and are oxidized to TiO_x clusters by the oxygen released in this reaction.

a)

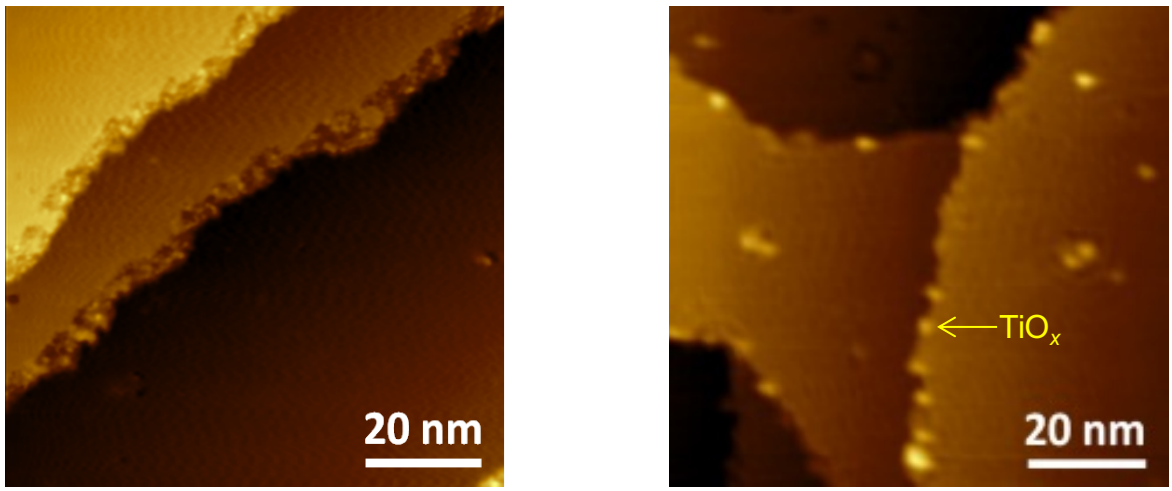

b)

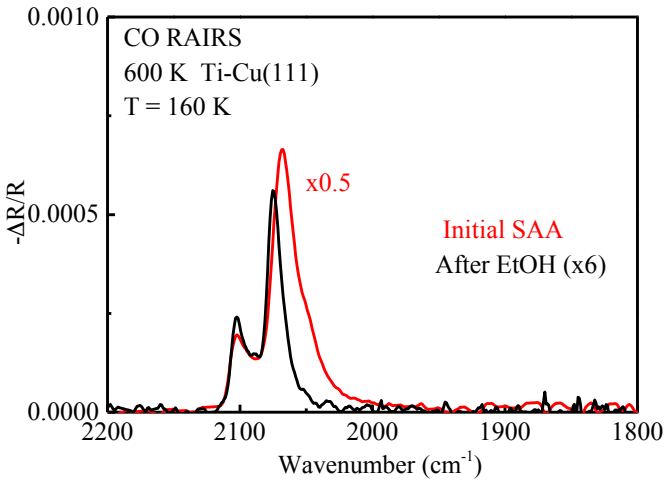

Figure 5. a) STM images obtained from a Ti-Cu(111) SAA before (left) and after (right) six successive ethanol TPRS experiments. Clusters attributed to TiO_x, formed via ethanol deoxygenation on Ti sites, are highlighted in the image on the right. b) CO RAIRS spectra acquired at 160 K before and after repeated (6x) ethanol TPRS on the Ti-Cu(111) SAA.

Computational results

DFT predicts that ethanol deoxygenation to gaseous ethylene and H_2 is energetically favorable on Ti-Cu(111) surface alloys. Figure 6 shows an energy diagram and molecular structures for ethanol reaction pathways computed for the Ti_1-Cu(111) surface, where one Ti atom substitutes one Cu atom in the surface layer. The calculations predict that adsorbed ethanol will readily deprotonate to

generate co-adsorbed ethoxy and H on the Ti_1 site as the barriers for ethanol desorption and deprotonation are 1.41 eV and 0.33 eV, respectively. The subsequent reactions of adsorbed ethoxy were investigated after removing the H-atom from the surface because this reaction step is facile, requiring only 0.35 eV in internal energy to generate ½ moles of H_2(g). As seen in Figure 6, ethoxy can undergo dehydrogenation to adsorbed acetaldehyde and a H-atom or deoxygenation to generate an adsorbed ethyl group and an O-atom. The ethoxy C-H bond cleavage step has a barrier of 1.24 eV and the reaction is endothermic by 0.62 eV. The resulting acetaldehyde product bonds strongly to the Ti_1 site through its O-atom, achieving a binding energy of 2.22 eV.

Ethoxy C-O bond cleavage has a barrier of 1.72 eV and is thermoneutral on the Ti_1 site. The O-atom released in this step binds to a hollow site comprised of the Ti atom and two Cu atoms, while the ethyl product is positioned on the opposing side of the Ti atom (Figure 6). The production of gaseous ethylene then involves dehydrogenation of the ethyl group followed by ethylene desorption for which the barriers are 0.52 eV and 0.98 eV, respectively. An alternate pathway for C_2H_4 formation is the conversion of CH_3CHO to a CH_2CH_2O species, followed by C-O cleavage. However, DFT suggests that this route is improbable on the Ti_1 site as the energy of the CH_2CH_2O intermediate is about 0.55 eV above the CH_3CHO state. From the Brønsted-Evans-Polanyi (BEP) relation, the transition states for CH_2CH_2O formation and subsequent C-O cleavage will lie even higher in energy, likely reaching values well above the transition state for ethoxy C-O cleavage.

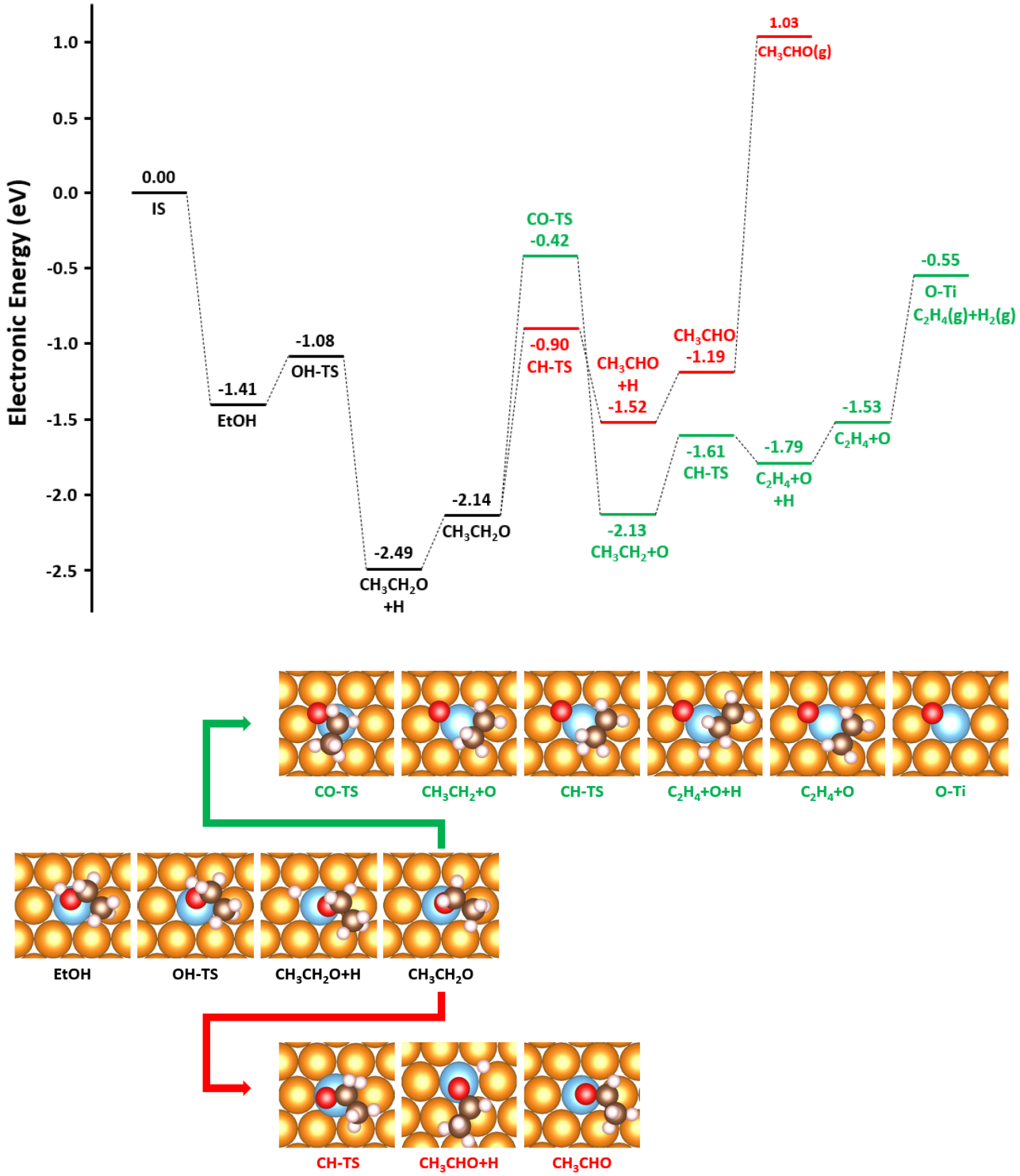

Figure 6. (a) Electronic energy profile (eV) for ethanol deoxygenation (green) and dehydrogenation (red) on Ti_1-Cu(111) (the common part is in black). TS indicates transition states. All species are chemisorbed unless specifically noted by (g) for gas phase species. (b) Corresponding atomic structures for intermediates and transition states. Color codes used in (b): Cu-light brown, Ti-blue, O-red, C-dark brown, H-light pink.

We find that ethoxy C-O bond cleavage is unlikely to take place on Ti-Cu subsurface alloys. DFT results show that the energy difference between the "CH_3CH_2 + O" state and ethoxy on Ti_3-Cu(111) capped by a monolayer of inert Cu is as high as +0.67 eV. The activation barrier for this step on such a surface is hence expected to be much higher than that of 1.72 eV on Ti_1-Cu(111), based on the BEP relation. As a result, ethanol deoxygenation is expected to occur negligibly on Ti-Cu subsurface alloys, consistent with experimental data discussed above.

The kinetic branching between ethoxy dehydrogenation and deoxygenation is challenging to infer from the energy diagram alone due to competing rate processes. Ethoxy C-H cleavage has a lower barrier than C-O cleavage (1.24 vs. 1.72 eV), suggesting that acetaldehyde formation will be kinetically favored on Ti_1 sites. However, the barrier for acetaldehyde hydrogenation is also lower than that of ethyl oxygenation (0.62 vs. 1.71 eV), and the acetaldehyde desorption barrier is high. As such, rather than desorbing, the adsorbed acetaldehyde can be hydrogenated to regenerate ethoxy, which can subsequently react by the deoxygenation pathway. As shown below, kinetic simulations were performed to clarify the rates and branching of ethanol reactions on Ti-Cu(111) alloy surfaces during TPRS.

Enhancement of ethanol deoxygenation with increasing Ti ensemble size

The chemical reactivity of the Ti_n ensembles toward ethanol increases significantly as the ensemble size is increased from n = 1 to 3, with the most dramatic enhancement occurring between Ti monomers and dimers. A triangular configuration is considered for the Ti trimer. The barrier for ethanol O-H cleavage is already low on the Ti_1 site at 0.33 eV, but decreases even more to 0.16 eV on

the Ti_2 site and O-H cleavage is a barrierless process on Ti_3. A particularly pronounced effect is that the barriers for ethoxy C-H and C-O bond cleavage are 0.55 eV and 0.64 eV, respectively, lower on a Ti dimer compared with the monomer (Table 1), demonstrating that the Ti_2 site is more reactive than the Ti_1 site toward ethoxy. A difference is that the barrier for acetaldehyde hydrogenation is 0.35 eV lower, whereas the barrier for ethyl oxygenation is slightly higher on the Ti_2 vs. Ti_1 site. These opposing changes, in addition to enhanced stabilization of acetaldehyde on the Ti dimer (Table 1, Fig. S3), increase the selectivity for ethoxy deoxygenation to ethylene on the Ti_2 site compared with the Ti_1 site. The barriers for both ethyl dehydrogenation and ethylene desorption are also slightly lower on the Ti_2 vs. Ti_1 site, further favoring ethylene production (Table 1, Fig. S3). Thus, increasing the Ti ensemble size from monomer to dimer enhances the chemical activity and selectivity toward ethanol deoxygenation to ethylene and H_2.

Table 1. Reaction steps and the forward (E_f) and reverse (E_r) energy barriers determined from DFT for ethanol adsorbed on Ti_n ensembles of varying size (n = 1, 2, 3) in Ti-Cu(111) alloy surfaces. Desorption steps are treated as irreversible to simulate TPRS conditions so reverse barriers for these steps are omitted, as indicated by the symbol "---". Energies are given in unit of eV. *Adsorbed ethanol deprotonated spontaneously on the Ti_3 ensemble during relaxation so the value of E_r for the ethanol dehydrogenation step represents the barrier for ethoxy + H to convert to a gaseous ethanol molecule.

Reaction	**Equation**	Ti_1		Ti_2		Ti_3	
		E_f	E_r	E_f	E_r	E_f	E_r
Ethanol desorption	$CH_3CH_2OH \rightarrow CH_3CH_2OH(g)$	1.41	---	1.3	---	---	---
Ethanol dehydrogenation	$CH_3CH_2OH \rightleftharpoons CH_3CH_2O + H$	0.33	1.41	0.16	1.67	---	3.21*
Ethoxy dehydrogenation	$CH_3CH_2O \rightleftharpoons CH_3CHO + H$	1.24	0.62	0.69	0.27	0.91	0.85
Acetaldehyde desorption	$CH_3CHO \rightarrow CH_3CHO(g)$	2.22	---	2.79	---	3.19	---
Ethoxy deoxygenation	$CH_3CH_2O \rightleftharpoons CH_3CH_2 + O$	1.72	1.71	1.08	1.78	0.8	1.9
Ethyl dehydrogenation	$CH_3CH_2 + O \rightleftharpoons C_2H_4 + O + H$	0.52	0.18	0.44	0.23	0.7	0.45
Ethylene desorption	$C_2H_4 + O \rightarrow C_2H_4(g) + O$	0.98	---	0.75	---	0.83	---
Hydrogen desorption	$2H \rightarrow H_2(g)$	0.84	---	1.01	---	1.0	---

Increasing the Ti ensemble size from Ti_2 to Ti_3 further increases the activity and selectivity for

ethanol deoxygenation. The barrier for ethoxy dehydrogenation is 0.22 eV higher, whereas the ethoxy deoxygenation barrier is 0.28 eV lower on the Ti_3 vs. Ti_2 site (Table 1, Fig. S3, S4). The net effect is that the ethoxy C-O cleavage barrier is about 0.1 eV lower than the C-H cleavage barrier on the Ti_3 site. Although the acetaldehyde hydrogenation barrier is also higher on the Ti_3 vs. Ti_2 site, kinetic simulations show that deoxygenation remains favored because the barrier for ethoxy C-O cleavage is lower than that for C-H cleavage (see below). The improved activity and selectivity for ethanol deoxygenation arises partly from enhanced stabilization of the O-atom product on the Ti_2 and Ti_3 ensembles. On the Ti_1 site, the O-atom released from ethoxy bonds with the Ti atom and two Cu atoms in a threefold hollow site (Fig. 6). Compared with the Ti_1 site, the O-atom coordinates with more Ti atoms on the larger ensembles (Ti_2 bridge site vs. Ti_3 hollow site, Fig. S3 and S4) and thereby achieves stronger bonding since Ti is more oxophilic than Cu; DFT estimates that the O binding energies on the Ti_2 and Ti_3 ensembles are 1.2 and 1.9 eV stronger than on Ti_1, respectively. In accord with the BEP relation, this stabilization of the final state lowers the barrier for ethoxy C-O cleavage, resulting in an enhancement in ethanol deoxygenation activity as the Ti_n ensemble size increases from n = 1 to 3.

TPRS simulations

A microkinetic model was developed based on the reaction steps and energies predicted by DFT and applied to simulate TPRS traces that evolve after ethanol adsorption on Ti-Cu(111) alloys with different Ti ensemble sizes. Table 1 lists the elementary steps and reaction barriers included in the model and more details are given in SI, section S5. Following recent work, our treatment of H_2 associative desorption assumes that H-atoms can migrate rapidly between Ti ensembles, and that the

dissociation barrier of gaseous H_2 is 0.23 eV, independent of ensemble size.[20]

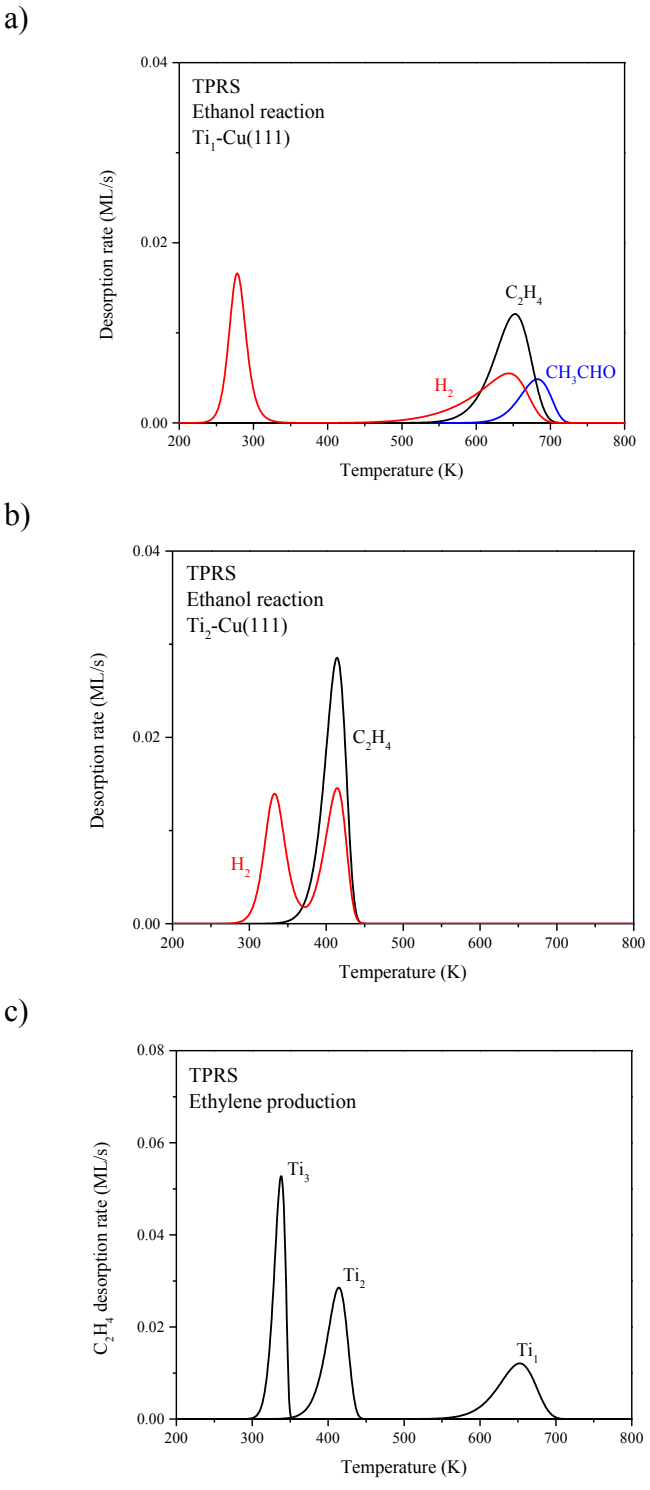

Figure 7. Simulated TPRS spectra of reaction products that evolve from ethanol reactions on (a) a Ti_1 site and (b) a Ti_2 ensemble in Ti-Cu(111) alloy surfaces. (c) TPRS traces of the C_2H_4 product resulting from ethanol deoxygenation on Ti_1, Ti_2 and Ti_3 ensembles in Ti-Cu(111).

The TPRS simulations reinforce the conclusion that the ethanol deoxygenation activity and selectivity increase with increasing Ti ensemble size from n = 1 to 3. The simulations predict that all of the ethanol adsorbed on the Ti ensembles reacts rather than desorbing because the ethanol desorption barrier is considerably higher than both the deprotonation barrier and the H_2 desorption barrier (Table 1). For the Ti_1 site, the simulations predict a desorption-limited H_2 TPRS peak near 280 K where the H-atoms originate from ethanol deprotonation at lower temperature (Figure 7). Thereafter, H_2 desorbs in a broader, reaction-limited feature at ~645 K, while C_2H_4 and CH_3CHO desorb nearly concurrently in peaks at 650 K and 680 K, respectively. The C_2H_4 TPRS yield is equal to about 75% of the initially adsorbed ethanol, demonstrating higher selectivity for ethanol deoxygenation over dehydrogenation on the Ti_1 site. Analogous behavior is predicted for ethanol reactions on the Ti_2 site in that a desorption-limited H_2 peak near 330 K precedes the evolution of C_2H_4 and H_2 in peaks near 410 K (Figure 7b). However, the Ti_2 ensemble is more active and selective toward ethanol deoxygenation than the Ti_1 site. All of the adsorbed ethanol converts to gaseous ethylene on the Ti_2 ensemble and the C_2H_4 desorption temperature is 240 K lower on Ti_2 vs. Ti_1 (Figure 7a-b). The Ti_3 ensemble also exhibits 100% selectivity toward ethanol deoxygenation and is more active than the Ti_2 ensemble as the C_2H_4 TPRS peak emerges near 340 K (Figure 7c, S5).

Comparison between experimental and simulated TPRS traces suggests that Ti_2 and Ti_3 ensembles are primarily responsible for the ethanol reactivity observed experimentally. The main reason for this conclusion is that the C_2H_4 and reaction-limited H_2 TPRS features predicted for the Ti_2 and Ti_3 ensembles evolve within a similar temperature range as observed experimentally (~300-500 K) for the initially metallic Ti-Cu(111) surfaces. In contrast, simulations of ethanol

reaction on the Ti_1 site predict product desorption at temperatures (>~ 600 K) that are considerably greater than those at which products evolved from the initial metallic surfaces in the experiments. Given that Ti_1 sites are present on the Ti-Cu(111) alloy surfaces studied experimentally,[19] we speculate that complete decomposition of the adsorbed reaction products ensues at temperatures (~600 K) lower than that needed for their desorption from these sites. Notably, the simulations predict distinct desorption- and reaction-limited H_2 TPRS features, whereas different H_2 TPRS peaks were not resolved in the experimental data. This difference between simulation and experiment has no effect on the main conclusions, and likely reflects heterogeneity in the Ti ensemble sizes present on the experimentally-studied Ti-Cu(111) surfaces and possibly slight underestimation of the H_2 recombination rates in the simulations. The key finding is that the TPRS spectra simulated for ethanol reaction on the Ti_2 and Ti_3 ensembles agree well with experimental data, demonstrating a strong effect of Ti ensemble size and suggesting that reaction on Ti dimers and trimers is mainly responsible for the high activity and selectivity for ethanol deoxygenation to ethylene and H_2 observed experimentally.

Facilitation of C_2H_4 desorption by O(ad)

The DFT calculations predict that C_2H_4 desorption from the Ti ensembles is significantly promoted by the adsorbed O atom that is generated during the ethoxy deoxygenation step. This behavior demonstrates that an adsorbed reaction product alters the chemical properties of the small Ti ensembles in a way that enhances the reaction selectivity toward desired products. To ascertain the effects of the adsorbed O-atom, we computed the energies of adsorbed C_2H_4 and its dehydrogenation

product (C_2H_3 + H) for Ti ensembles with vs. without an adsorbed O-atom. Here, the destabilization energy ($E_{O\text{-}clean}$) of an adsorbed species is defined as the difference in energy between the adsorbed species on a Ti ensemble with vs. without an adsorbed O-atom, e.g., $E_{O\text{-}clean}(C_2H_4) = E(C_2H_4$ w/ O) – $E(C_2H_4$ on clean Ti) while the net destabilization energy is equal to the difference in destabilization energies of the C_2H_3 + H and C_2H_4 species, i.e., $\Delta E = E_{O\text{-}clean}(C_2H_3 + H) - E_{O\text{-}clean}(C_2H_4)$. A positive value of the net destabilization energy (ΔE) means that the dehydrogenation product is destabilized to a greater extent than C_2H_4 and thus that C_2H_4 desorption is energetically favored over dehydrogenation when O is present. Our results show that both the C_2H_4 and C_2H_3 + H states have higher energies (i.e., lower stability) on Ti ensembles with vs. without an adsorbed O-atom, and that the C_2H_3 + H state is destabilized to a greater extent than the C_2H_4 species (Table 2). Destabilization of C_2H_4 facilitates its desorption while the larger destabilization of the C_2H_3 + H state suppresses C_2H_4 dehydrogenation, acting to further promote C_2H_4 desorption over dehydrogenation.

Table 2. Electronic energies of C_2H_4 and C_2H_3 + H adsorbed on Ti_n ensembles (n = 1 to 3) with ("*w/ O*") vs. without ("*clean*") a co-adsorbed O-atom, with the reference energy taken as the energy of an isolated C_2H_4 molecule plus the Ti_n-Cu(111) surface with or without an adsorbed O-atom. The first two entries in each column labeled as "$E_{O\text{-}clean}$" are equal to the difference in energy of the adsorbed species on clean Ti_n vs. Ti_n with an adsorbed O-atom, i.e., $E_{O\text{-}clean} = E_O$(species) – E_{clean}(species), and represent the destabilization energy of the species caused by the co-adsorbed O-atom. The bottom row labeled as "ΔE" represents the energy difference between the C_2H_3 + H and C_2H_4 states on clean Ti_n vs. Ti_n with an adsorbed O-atom, with the final entry in the ΔE row for each Ti_n structure equaling the difference $E_{O\text{-}clean}(C_2H_3 + H) - E_{O\text{-}clean}(C_2H_4)$, which is referred to as the net destabilization energy in the text.

Species	Ti_1			Ti_2			Ti_3		
	clean	*w/ O*	$E_{O\text{-}clean}$	*clean*	*w/ O*	$E_{O\text{-}clean}$	*clean*	*w/ O*	$E_{O\text{-}clean}$
C_2H_4	-1.23	-0.99	0.24	-1.93	-0.76	1.17	-2.28	-0.84	1.44
C_2H_3 + H	-0.79	-0.34	0.45	-1.80	-0.07	1.73	-2.34	0.14	2.48
ΔE	**0.44**	**0.65**	**0.21**	**0.13**	**0.69**	**0.56**	**-0.06**	**0.98**	**1.04**

Our results also reveal that adsorbed O produces larger enhancements in C_2H_4 desorption from Ti ensembles of increasing size from n = 1 to 3. Adsorbed O on the Ti_1 site destabilizes the C_2H_4 and C_2H_3 + H species by 0.24 eV and 0.45 eV, respectively, resulting in a net destabilization of ΔE = 0.21 eV (Table 2). For the Ti_2 and Ti_3 ensembles, the C_2H_4 destabilization energies by an adsorbed O-atom are $E_{O\text{-}clean}(C_2H_4)$ = 1.2 and 1.4 eV and the net destabilization energies are ΔE = 0.6 and 1.0 eV, respectively (Table 2). As mentioned above, stronger O-atom binding promotes ethanol deoxygenation on Ti ensembles of increasing size by stabilizing the final and transition states for ethoxy C-O bond cleavage. The present comparisons reveal that the presence of an adsorbed O-atom also promotes subsequent C_2H_4 desorption by destabilizing this species and its dehydrogenation product, and that this facilitation of C_2H_4 desorption is amplified as the Ti ensemble size increases.

We expect, however, that the preference for C_2H_4 desorption over dehydrogenation is limited to atomic-scale Ti ensembles. On larger ensembles, the C_2H_4 product can diffuse away from the adsorbed O-atom and reach Ti sites at which dehydrogenation is favored over desorption. For example, even on a Ti_3 ensemble, C_2H_4 dehydrogenation is slightly favored over desorption when an adsorbed O-atom is absent (Table 2). On a full Ti monolayer on Cu(111), C_2H_4 binds strongly (2.24 eV) and dehydrogenation is exothermic by about 1.1 eV, suggesting that the C_2H_4 product will tend to dehydrogenate rather than desorb when the Ti ensemble is sufficiently large. Overall, our results demonstrate that adsorbed O enhances C_2H_4 production from ethanol on Ti-Cu(111) surfaces and that this promotional effect is more pronounced on atomic-scale Ti ensembles of increasing size from n = 1 to 3.

Geometric and electronic influence of O(ad)

Adsorbed O affects the binding of C_2H_4 on Ti ensembles through both geometric and electronic effects. Ethylene achieves optimal binding at the Ti bridge and hollow sites of clean Ti_2 and Ti_3 ensembles, but O occupies these sites as well, forcing co-adsorbed C_2H_4 to move to hollow sites at the periphery of the ensembles where its binding is weaker (Fig. S6). Comparisons of the electronic density of states (DOS) also demonstrate that O adsorption on the Ti ensembles depletes Ti 3*d* states available for bonding with other adsorbates (Fig. S7). The loss of these Ti 3*d* states thus weakens the bonding of Ti with C_2H_4 and its dehydrogenation product (C_2H_3 + H), thereby further destabilizing these species and facilitating C_2H_4 desorption.

Discussion

Our results show that Ti-Cu(111) alloy surfaces are highly selective and active in promoting ethanol deoxygenation to ethylene and reveal that this chemistry is enhanced on atomic-scale Ti ensembles of increasing sizes and in the presence of the adsorbed O-atom product. Among the Ti ensembles investigated with DFT, the Ti_2 and Ti_3 ensembles are more active and selective than the Ti_1 site for ethanol deoxygenation, while the calculations also provide evidence that ethylene production will diminish on Ti ensembles that are sufficiently large because the C_2H_4 product will decompose on such structures. An implication is that a Ti_n ensemble size of n = 2 or 3 is likely optimal for achieving efficient ethanol deoxygenation to C_2H_4 on Ti-Cu(111) surfaces. Future efforts to atomically resolve small Ti_n ensembles in Cu(111) using STM and characterize surfaces with varying Ti concentration

could further advance the understanding of how the ethanol reactivity is influenced by the Ti ensemble size. Increased oxygen adsorption strengths are mainly responsible for the enhancement in ethanol deoxygenation activity as the Ti ensemble size increases from monomer to trimer. Formation of more strongly-bound O on the Ti ensembles causes both increased stability of the transition and final states for ethoxy C-O bond cleavage and greater destabilization of the subsequent C_2H_4 product, with these effects acting to accentuate the conversion of ethanol to ethylene. The strong influence of the adsorbed O-atom product on the reaction steps following C-O cleavage is a particularly interesting phenomenon that may have broad implications for understanding the chemical behavior of atomic-scale ensembles in alloy catalysts.

A challenge in utilizing dilute Ti-Cu alloys for ethanol conversion to ethylene under catalytic conditions is that the adsorbed O-atoms need to be removed to regenerate the active Ti sites. Consistent with activated H_2 dissociation, we find that under UHV conditions H_2 dissociates negligibly on the initial Ti-Cu(111) surfaces and is ineffective in removing the surface oxygen generated by ethanol deoxygenation. However, a recent study shows that H_2 dissociative adsorption occurs efficiently over nanoporous TiCu at ambient pressures, resulting in facile H_2-D_2 exchange at temperatures between 323 and 523 K.[20] Furthermore, oxidized Ti moieties at the surface of the nanoporous TiCu could be reduced to the metallic state during exposure of the catalysts to ~100 mTorr of H_2 at temperatures between 523 and 673 K. The difference in H_2 reactivity on Ti-Cu surfaces in UHV vs. higher pressures is consistent with predictions that H_2 dissociation is activated on Ti-Cu(111) surfaces but that the barrier is only ~0.2 eV.[20] Thus, the catalytic conversion of ethanol to ethylene may occur efficiently over Ti-Cu catalysts at ambient pressures because higher fluxes of

gaseous H_2 would be available to abstract the adsorbed O generated during reaction, producing H_2O and regenerating active Ti sites.

Summary

Metallic Ti-Cu(111) surfaces with small Ti concentrations (~0.10 ML) are highly active and selective toward the deoxygenation of ethanol. A surface with Cu-capped, Ti-containing islands as well as a dilute Ti-Cu(111) alloy each promote the deoxygenation of adsorbed ethanol to C_2H_4 and H_2 during TPRS, with these reaction products desorbing near 400 K from both surfaces. The Ti sites become oxidized to TiO_x by the oxygen released during ethanol deoxygenation, causing the ethanol selectivity to change from C_2H_4 to CH_3CHO production after repeated ethanol TPRS experiments. Changes in the surface structure further confirm that TiO_x forms during ethanol TPRS on the Ti-Cu(111) alloy, subsuming single-atom Ti sites, and strongly suggest that ethanol reacts on the island-covered surface only at a small fraction of Ti sites that are exposed at the vacuum-solid interface, with the subsurface Ti sites remaining inactive.

DFT calculations confirm that Ti ensembles in a Ti-Cu(111) surface alloy promote the deoxygenation of ethanol to C_2H_4 and H_2 at moderate temperatures during TPRS, and predict that the activity and selectivity toward these products is significantly increased with increasing Ti ensemble size from n = 1 to 3. The enhanced activity for C_2H_4 production as the Ti ensemble size is increased arises from stabilization of the adsorbed O-atom released during C-O bond cleavage as well as destabilization of C_2H_4 and its dehydrogenation product when O is present on the Ti ensembles. The calculations further suggest that the low nuclearity of Ti dimers and trimers suppresses the complete

decomposition of ethanol and is thus important for gaseous C_2H_4 production. Our results demonstrate that dilute Ti-Cu(111) alloys are highly selective in promoting the deoxygenation of ethanol to C_2H_4 at moderate temperature (~400 K) and provide insights for understanding how the Ti ensemble size and the adsorbed O-atom product influence reactivity.

Supporting Information

Ethanol TPRS from sputtered vs. annealed Cu(111); Effects of thermal annealing on CO RAIRS from Ti-Cu(111); Energy diagram and molecular structures for ethanol reactions on Ti_2-Cu(111); Energy diagram and molecular structures for ethanol reactions on Ti_3-Cu(111); TPRS simulations of ethanol on Ti_n-Cu(111); Configurations of C_2H_4 adsorbed on Ti_n-Cu(111) with vs. without an adsorbed O atom; Electronic density of states of Ti_n-Cu(111) surfaces with vs. without O(ad)

Acknowledgements

We dedicate this work to the late Professor Robert J. Madix and express our deepest gratitude for his guidance and inspiration over the years. This work was supported as part of the Integrated Mesoscale Architectures for Sustainable Catalysis, an Energy Frontier Research Center funded by the U.S. Department of Energy, Office of Science, Basic Energy Sciences under Award No. DE-SC0012573. DFT calculations reported in this work used computational and storage resources on the Hoffman2 cluster at the UCLA Institute for Digital Research and Education (IDRE), the National Energy Research Scientific Computing Center (NERSC) of the U.S. Department of Energy, and the Bridges-2 cluster through the allocation CHE170060 at the Pittsburgh Supercomputing Center

through ACCESS.

References

1. Giannakakis, G.; Flytzani-Stephanopoulos, M.; Sykes, E. C. H., Single-Atom Alloys as a Reductionist Approach to the Rational Design of Heterogeneous Catalysts, *Acc. Chem. Res.* **2019,** 52, 237-247.
2. Hannagan, R. T.; Giannakakis, G.; Flytzani-Stephanopoulos, M.; Sykes, E. C. H., Single-atom alloy catalysts, *Chem. Rev.* **2020,** 120, 12044–12088.
3. Greiner, M. T.; Jones, T. E.; Beeg, S.; Zwiener, L.; Scherzer, M.; Girgsdies, F.; Piccinin, S.; Armbruster, M.; Knop-Gericke, A.; Schlogl, R., Free-atom-like d states in single-atom alloy catalysts, *Nature Chem.* **2018,** 10, 1008-1015.
4. Fung, V.; Hu, G. X.; Sumpter, B., Electronic band contraction induced low temperature methane activation on metal alloys, *J. Mater. Chem. A* **2020,** 8, 6057-6066.
5. Darby, M. T.; Stamatakis, M.; Michaelides, A.; Sykes, E. C. H., Lonely Atoms with Special Gifts: Breaking Linear Scaling Relationships in Heterogeneous Catalysis with Single-Atom Alloys, *J. Phys. Chem. Lett.* **2018,** 9, 5636-5646.
6. Marcinkowski, M. D.; Darby, M. T.; Liu, J. L.; Wimble, J. M.; Lucci, F. R.; Lee, S.; Michaelides, A.; Flytzani-Stephanopoulos, M.; Stamatakis, M.; Sykes, E. C. H., Pt/Cu single-atom alloys as coke-resistant catalysts for efficient C-H activation, *Nature Chem.* **2018,** 10, 325-332.
7. Lucci, F. R.; Lawton, T. J.; Pronschinske, A.; Sykes, E. C. H., Atomic Scale Surface Structure of Pt/Cu(111) Surface Alloys, *J. Phys. Chem. C* **2014,** 118, 3015-3022.
8. Lucci, F. R.; Liu, J. L.; Marcinkowski, M. D.; Yang, M.; Allard, L. F.; Flytzani-Stephanopoulos, M.; Sykes, E. C. H., Selective hydrogenation of 1,3-butadiene on platinum-copper alloys at the single-atom limit, *Nat. Commun.* **2015,** 6, 8550.
9. Hannagan, R. T.; Patel, D. A.; Cramer, L. A.; Schilling, A. C.; Ryan, P. T. P.; Larson, A. M.; Cinar, V.; Wang, Y. C.; Balema, T. A.; Sykes, E. C. H., Combining STM, RAIRS and TPD to Decipher the Dispersion and Interactions Between Active Sites in RhCu Single-Atom Alloys, *Chemcatchem* **2020,** 12, 488-493.
10. Therrien, A. J.; Hensley, A. J. R.; Marcinkowski, M. D.; Zhang, R. Q.; Lucci, F. R.; Coughlin, B.; Schilling, A. C.; McEwen, J. S.; Sykes, E. C. H., An atomic-scale view of single-site Pt catalysis for low-temperature CO oxidation, *Nature Catalysis* **2018,** 1, 192-198.
11. Cao, X. R.; Ji, Y. F.; Luo, Y., Dehydrogenation of Propane to Propylene by a Pd/Cu Single-Atom Catalyst: Insight from First-Principles Calculations, *J. Phys. Chem. C* **2015,** 119, 1016-1023.
12. Kruppe, C. M.; Krooswyk, J. D.; Trenary, M., Polarization-Dependent Infrared Spectroscopy of Adsorbed Carbon Monoxide To Probe the Surface of a Pd/Cu(111) Single-Atom Alloy, *J. Phys. Chem. C* **2017,** 121, 9361-9369.
13. Luneau, M.; Lim, J. S.; Patel, D. A.; Sykes, E. C. H.; Friend, C. M.; Sautet, P., Guidelines to Achieving High Selectivity for the Hydrogenation of alpha,beta-Unsaturated Aldehydes with Bimetallic and Dilute Alloy Catalysts: A Review, *Chem. Rev.* **2020,** 120, 12834-12872.
14. Qu, L.; Jiang, X.; Zhang, Z. H.; Zhang, X. G.; Song, G. Y.; Wang, H. L.; Yuan, Y. P.; Chang, Y. L., A review of hydrodeoxygenation of bio-oil: model compounds, catalysts, and equipment, *Green Chem.* **2021,** 23, 9348-9376.
15. Gan, T.; Liu, Y. F.; He, Q.; Zhang, H.; He, X. H.; Ji, H. B., Facile Synthesis of Kilogram-Scale Co-Alloyed Pt Single-Atom Catalysts via Ball Milling for Hydrodeoxygenation of 5-Hydroxymethylfurfural, *Acs Sustainable Chemistry & Engineering* **2020,** 8, 8692-8699.

16. Zhou, J. W.; An, W.; Wang, Z. M.; Jia, X., Hydrodeoxygenation of phenol over Ni-based bimetallic single-atom surface alloys: mechanism, kinetics and descriptor, *Catal. Sci. Tech.* **2019,** 9, 4314-4326.

17. Jia, X.; An, W.; Wang, Z. M.; Zhou, J. W., Effect of Doped Metals on Hydrodeoxygenation of Phenol over Pt-Based Bimetallic Alloys: C-aryl-OH Versus CaliphaticH-H Bond Scission, *J. Phys. Chem. C* **2019,** 123, 16873-16882.

18. Kress, P. L.; Zhang, S. J.; Wang, Y. C.; Cinar, V.; Friend, C. M.; Sykes, E. C. H.; Montemore, M. M., A Priori Design of Dual-Atom Alloy Sites and Experimental Demonstration of Ethanol Dehydrogenation and Dehydration on PtCrAg, *J. Am. Chem. Soc.* **2023,** 145, 8401-8407.

19. Shi, J. J.; Owen, C. J.; Ngan, H. T.; Qin, S. Y.; Mehar, V.; Sautet, P.; Weaver, J. F., Formation of a Ti-Cu(111) single atom alloy: Structure and CO binding, *J. Chem. Phys.* **2021,** 154, 234703.

20. Lee, J. D.; Qi, Z.; Foucher, A. C.; Ngan, H. T.; Dennis, K.; Cui, J.; Sadykov, I. I.; Crumlin, E. J.; Sautet, P.; Stach, E. A.; Friend, C. M.; Madix, R. J.; Biener, J., Facilitating Hydrogen Dissociation over Dilute Nanoporous Ti-Cu Catalysts, *J. Am. Chem. Soc.* **2022,** 144, 16778–16791.

21. Zhang, F.; Pan, L.; Li, T.; Diulus, J.; Asthagiri, A.; Weaver, J. F., CO oxidation on PdO(101) during temperature programmed reaction spectroscopy: Role of oxygen vacancies, *J. Phys. Chem. C* **2014,** 118, 28647–28661.

22. Mehar, V.; O'Connor, C. R.; Egle, T.; Karatok, M.; Madix, R. J.; Friend, C. M.; Weaver, J. F., Growth and auto-oxidation of Pd on single-layer AgO_x/Ag(111), *Phys. Chem. Chem. Phys.* **2020,** 22, 6202-6209.

23. Davis, L. E. M., N.C.; Palmberg, P.W.; Riach, G.E.; Weber, R.E., *Handbook of Auger Electron Spectroscopy*. Physical Electronics Division, Perkin Elmer Corporation: Eden Praire, MN, 1976; p 1-253.

24. Kresse, G.; Hafner, J., Ab-initio molecular-dynamics simulation of the liquid-metal amorphous-semiconductor transition in germanium, *Phys. Rev. B* **1994,** 49, 14251-14269.

25. Kresse, G.; Furthmuller, J., Efficient iterative schemes for ab initio total-energy calculations using a plane-wave basis set, *Phys. Rev. B* **1996,** 54, 11169-11186.

26. Kresse, G.; Furthmuller, J., Efficiency of ab-initio total energy calculations for metals and semiconductors using a plane-wave basis set, *Comp. Mater. Sci.* **1996,** 6, 15-50.

27. Kresse, G.; Hafner, J., Abinitio Hellmann-Feynman molecular-dynamics for liquid-metals, *J. Non-Cryst. Solids* **1993,** 156, 956-960.

28. Perdew, J. P.; Burke, K.; Ernzerhof, M., Generalized gradient approximation made simple, *Phys. Rev. Lett.* **1996,** 77, 3865.

29. Steinmann, S. N.; Corminboeuf, C., Comprehensive Bench marking of a Density-Dependent Dispersion Correction, *J. Chem. Theory Comput.* **2011,** 7, 3567-3577.

30. Maintz, S.; Deringer, V. L.; Tchougreeff, A. L.; Dronskowski, R., LOBSTER: A Tool to Extract Chemical Bonding from Plane-Wave Based DFT, *J. Comput. Chem.* **2016,** 37, 1030-1035.

31. Henkelman, G.; Uberuaga, B. P.; Jonsson, H., A climbing image nudged elastic band method for finding saddle points and minimum energy paths, *J. Chem. Phys.* **2000,** 113, 9901-9904.

32. Henkelman, G.; Jonsson, H., A dimer method for finding saddle points on high dimensional potential surfaces using only first derivatives, *J. Chem. Phys.* **1999,** 111, 7010-7022.

33. Momma, K.; Izumi, F., VESTA 3 for three-dimensional visualization of crystal, volumetric and morphology data, *J. Appl. Crystallogr.* **2011,** 44, 1272-1276.

34. Eren, B.; Liu, Z. Y.; Stacchiola, D.; Somorjai, G. A.; Salmeron, M., Structural Changes of Cu(110) and Cu(110)-(2 x 1)-O Surfaces under Carbon Monoxide in the Torr Pressure Range Studied with Scanning Tunneling Microscopy and Infrared Reflection Absorption Spectroscopy, *J. Phys. Chem. C* **2016,** 120, 8227-8231.

35. Roiaz, M.; Falivene, L.; Rameshan, C.; Cavallo, L.; Kozlov, S. M.; Rupprechter, G., Roughening of Copper (100) at

Elevated CO Pressure: Cu Adatom and Cluster Formation Enable CO Dissociation, *J. Phys. Chem. C* **2019,** 123, 8112-8121.

36. Mudiyanselage, K.; Xu, F.; Hoffmann, F. M.; Hrbek, J.; Waluyo, I.; Boscoboinik, J. A.; Stacchiola, D. J., Adsorbate-driven morphological changes on Cu(111) nano-pits, *Phys. Chem. Chem. Phys.* **2015,** 17, 3032-3038.

37. Hoffmann, F. M., Infrared reflection-absorption spectroscopy of adsorbed molecules *Surf. Sci. Rep.* **1983,** 3, 107-192.

38. Wang, Z. T.; Xu, Y. F.; El-Soda, M.; Lucci, F. R.; Madix, R. J.; Friend, C. M.; Sykes, E. C. H., Surface Structure Dependence of the Dry Dehydrogenation of Alcohols on Cu(111) and Cu(110), *J. Phys. Chem. C* **2017,** 121, 12800-12806.

39. Petrik, N. G.; Kimmel, G. A., Adsorption Geometry of CO versus Coverage on TiO_2(110) from s- and p-Polarized Infrared Spectroscopy, *J. Phys. Chem. Lett.* **2012,** 3, 3425-3430.

40. Boyle, D. T.; Wilke, J. A.; Palomino, R. M.; Lam, V. H.; Schlosser, D. A.; Andahazy, W. J.; Stopak, C. Z.; Stacchiola, D. J.; Rodriguez, J. A.; Baber, A. E., Elucidation of Active Sites for the Reaction of Ethanol on TiO2/Au(111), *J. Phys. Chem. C* **2017,** 121, 7794-7802.

Toc graphic

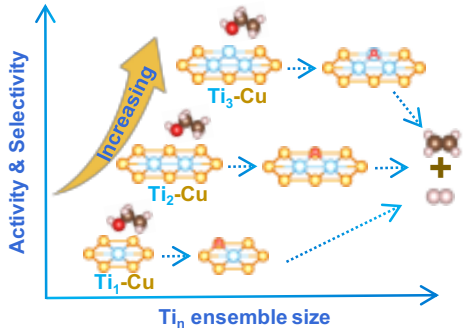
Activity & Selectivity
Increasing
Ti3-Cu
Ti2-Cu
Ti1-Cu
Tin ensemble size